Phase-space structure in plasma turbulence

Hideo Sugama, Tomohiko Watanabe

Phase-Space Structure in Plasma Turbulence

H. Sugama and T.-H. Watanabe

National Institute for Fusion Science / Graduate University for Advanced Studies

Toki 509-5292, Japan

Abstract

Plasma turbulence driven by the ion temperature gradient (ITG) is theoretically studied with high-resolution Eulerian kinetic simulations. A spectral analysis of the velocity distribution function in the slab ITG turbulence clarifies how the entropy variable associated with the fine-scale structure of the distribution function is produced by the turbulent heat transport in the presence of the temperature gradient, transferred from macro to microscales in the velocity space through phase-mixing processes, and dissipated by collisions. The entropy spectral function is analytically derived and confirmed by the simulation result. It is shown that the entropy spectrum obeys a power law in the range that is free from instability sources and collisional dissipation. The Eulerian gyrokinetic simulation of the toroidal ITG turbulence yields the ion thermal diffusivity in the steady turbulent state, in which the balance between the entropy production by the ion thermal transport and the collisional dissipation is verified. A formula for a long time behavior of the zonal flow potential in helical systems is analytically derived, by which collisionless zonal flow dynamics in tokamaks and helical plasmas are compared. A good agreement between the formula and the gyrokinetic simulation results is obtained.

1. INTRODUCTION

Plasma turbulence and resultant anomalous transport have long been a key issue in the magnetic fusion research. Complexity of the issue partly lies in the fact that, for qualitative study of turbulence in high-temperature plasmas, we should take account of kinetic characteristics and accordingly treat not only real-space but also velocity-space structures of the particle distribution function. Because of large computer memory and time required for calculation of the distribution function in such turbulent kinetic systems, detailed researches of its velocity-space structures in turbulent states have not much been made so far compared with those on the real-space structures of fluid variables. Such information on the velocity distribution is critically important for establishing a reliable kinetic-fluid model to predict turbulent transport coefficients quickly and accurately based on fluid simulations [1].

In the present work, combining high-resolution Eulerian kinetic simulation [2–4] with theoretical analysis, we investigate the velocity-space spectral structures in the ion temperature gradient (ITG) driven turbulence which causes anomalous transport in high-temperature plasmas [5]. This typical example of plasma turbulence involves a turbulent $\mathbf{E} \times \mathbf{B}$ flow and anomalous heat transport in the real space as well as phase-mixing and collisional dissipation processes in the velocity space.

We first consider the slab ITG turbulence in Sec. 2, where the entropy spectrum associated with turbulent fluctuations is theoretically derived by the spectral analysis of the velocity distribution function and compared with results from kinetic simulations which use a large enough number of grid points in the parallel velocity space to resolve phase-mixing processes [3]. It is shown that the entropy spectrum obeys a power law in the range that is free from instability sources and collisional dissipation.

The toroidal ITG turbulence is considered to be more relevant to anomalous transport observed in tokamaks and other devices such as helical systems. Then, gyrokinetic simulation results on anomalous transport and entropy balance in the toroidal ITG turbulence are presented in Sec. 3. Also, dynamics of zonal $\mathbf{E}\times\mathbf{B}$ flows, which critically influence the turbulent transport [6], is investigated for tokamaks and helical systems based on the gyrokinetic theory and simulation. We elucidate the velocity-space structures associated with the zonal flow dynamics and find how trapped particles in helical ripples are influential on the zonal flow damping.

2. SLAB ITG TURBULENCE

In this section, combining high-resolution Eulerian kinetic simulation with theoretical analysis, we elucidate the velocity-space spectral structures in the slab ITG turbulence.

2.1. Basic Kinetic Equation for Slab ITG Turbulence

Here, we consider a periodic two-dimensional slab configuration with translational symmetry in the z-direction, where the uniform magnetic field is set in the y-z plane such that $\mathbf{B} = B(\hat{z} + \theta\hat{y})$ with $\theta \ll 1$. Assuming the fluctuation part of the ion distribution function to be give by $\delta f_{\mathbf{k}}(v_\parallel, v_\perp) = \tilde{f}_{\mathbf{k}}(v_\parallel)F_M(v_\perp)$, with the Maxwellian velocity distribution F_M, neglecting the parallel nonlinear term and taking a $v_\perp$-integral of the ion gyrokinetic equation yield the following equation in the wave number space $\mathbf{k} = (k_x, k_y)$,

$$\begin{aligned}\partial_t\tilde{f}_{\mathbf{k}} + i\Theta v_\parallel k_y\tilde{f}_{\mathbf{k}} \quad &+ \quad \sum_{\mathbf{k}=\mathbf{k}'+\mathbf{k}''}\left(k'_y k''_x - k'_x k''_y\right)\Psi_{\mathbf{k}'}\tilde{f}_{\mathbf{k}''} \\ &= \quad -ik_y\Psi_{\mathbf{k}}\left[1 + (v_\parallel^2 - 1 - k^2)\eta_i/2 + \Theta v_\parallel\right]F_M(v_\parallel) + C_i(\tilde{f}_{\mathbf{k}}), \quad (1)\end{aligned}$$

where we also have assumed constant density and temperature gradients of the background ions in the x-direction with much larger scale-lengths [$L_n \equiv -d(\ln n)/dx$ and $L_T \equiv -d(\ln T_i)/dx$] than the fluctuation wave lengths. The electric potential $\phi_{\mathbf{k}}$ is related to $\Psi_{\mathbf{k}}$ by $\Psi_{\mathbf{k}} = e^{-k^2/2}\phi_{\mathbf{k}}$ with $k^2 = k_x^2 + k_y^2$. In addition to Eq. (1), the electron Boltzmann relation and the quasineutrality condition, which are not written here, are used to give a closed system of governing equations for the slab ITG turbulence [3]. In Eq. (1), we have used the following normalization; $x = x'/\rho_i$, $y = y'/\rho_i$, $v_\parallel = v'_\parallel/v_{ti}$, $t = t'v_{ti}/L_n$, $\tilde{f} = \tilde{f}'L_n v_{ti}/\rho_i n_0$, and $\phi = e\phi' L_n/T_i\rho_i$, where v_{ti}, ρ_i ($= v_{ti}/\Omega_i$), Ω_i, n_0, e, and T_i are the ion thermal velocity, the ion thermal gyro-radius, the ion gyrofrequency, the background plasma density, the elementary charge, and the background ion temperature ($T_i = m_i v_{ti}^2$; m_i means the ion mass), respectively. Prime means a dimensional quantity. Θ is defined as $\Theta = \theta L_n/\rho_i$. η_i is given by $\eta_i = L_n/L_T$.

The parallel advection term on the left hand side of Eq. (1) contributes to generation of fine-scale fluctuations of $\tilde{f}_{\mathbf{k}}$ in the velocity space, that is, the phase mixing. The instability drive is contained in the first group of terms on the right-hand side of Eq. (1). The last term on the right-hand side denotes the ion-ion collision term for which we employ the Lenard-Bernstein model collision operator, $C_i(\tilde{f}_{\mathbf{k}}) = \nu\partial_{v_\parallel}[\partial_{v_\parallel} + v_\parallel]\tilde{f}_{\mathbf{k}}(v_\parallel)$, with the collision frequency ν normalized by v_{ti}/L_n.

2.2. Spectral Analysis

In order to investigate the velocity-space structure of the distribution function, we expand $\tilde{f}_{\mathbf{k}}$ as

$$\tilde{f}_{\mathbf{k}}(v_\parallel) = \sum_{n=0}^{\infty} \hat{f}_{\mathbf{k},n} H_n(v_\parallel) F_M(v_\parallel), \tag{2}$$

where $H_n(v_\parallel)$ is the Hermite polynomial of order n. In terms of the coefficient $\hat{f}_{\mathbf{k},n}$ in the Hermite-polynomial expansion, Eq. (1) is rewritten by

$$\begin{aligned} &\frac{\partial \hat{f}_{\mathbf{k},n}}{\partial t} + ik_y\Theta\left[\hat{f}_{\mathbf{k},n-1} + (n+1)\hat{f}_{\mathbf{k},n+1}\right] + \sum_{\mathbf{k}=\mathbf{k}'+\mathbf{k}''}\left(k'_y k''_x - k'_x k''_y\right)\Psi_{\mathbf{k}'}\hat{f}_{\mathbf{k}'',n} \\ = \;& -ik_y\Psi_{\mathbf{k}}\left[\delta_{n,0}\left(1-\frac{\eta_i}{2}k^2\right) + \delta_{n,1}\Theta + \delta_{n,2}\frac{\eta_i}{2}\right], \end{aligned} \tag{3}$$

where $\delta_{n,m} = 1$ for $n = m$ and 0 for $n \neq m$. The phase mixing process associated with the parallel streaming of particles are now represented by the interaction to the adjacent-order [$(n-1)$ and $(n+1)$] terms in the Hermite-polynomial expansion of the perturbed distribution function with the same wave number vector $\mathbf{k}$ as shown in the second and third terms on the left-hand side of Eq. (3). On the other hand, the $\mathbf{E}\times\mathbf{B}$ convection, which is given by the last term on the left-hand side, involves the distribution functions of only the same order n but with different wave number vectors $\mathbf{k}''$. The linear source terms proportional to $\Psi_{\mathbf{k}}$ on the right-hand side disappear for $n \geq 3$, which is the reason why the Hermite-polynomial expansion is employed here. A clear cutoff of the source like this never occurs if we use the Fourier expansion in terms of $\exp(ilv_\parallel)$ $(-\infty < l < \infty)$ as basis functions.

We define the entropy variable δS by [7–9]

$$\delta S \equiv \sum_{\mathbf{k}} \int dv_\parallel \frac{\langle|\tilde{f}_{\mathbf{k}}|^2\rangle}{2F_M} \equiv \sum_n \sum_{\mathbf{k}} \frac{1}{2} n! \langle|\hat{f}_{\mathbf{k},n}|^2\rangle \equiv \sum_n \sum_{\mathbf{k}} \delta S_{\mathbf{k},n} \equiv \sum_n \delta S_n, \tag{4}$$

where $\delta S_{\mathbf{k},n} \equiv \frac{1}{2} n! \langle|\hat{f}_{\mathbf{k},n}|^2\rangle$ and $\delta S_n \equiv \sum_{\mathbf{k}} \delta S_{\mathbf{k},n}$ represent the entropy spectral functions in the $(\mathbf{k}, n)$-space and in the n-space, respectively, and $\langle\cdots\rangle$ denotes the ensemble average. Using Eq. (1), we obtain

$$\frac{d}{dt}\delta S_n = \eta_i Q_i \delta_{n,2} + J_{n-1/2} - J_{n+1/2} - 2\nu n \delta S_n \qquad \text{for } n \geq 2, \tag{5}$$

where

$$J_{n-1/2} \equiv \sum_{\mathbf{k}} \Theta k_y n! \mathrm{Im}\langle \hat{f}_{\mathbf{k},n-1} \hat{f}^*_{\mathbf{k},n}\rangle, \tag{6}$$

$$J_{n+1/2} \equiv \sum_{\mathbf{k}} \Theta k_y (n+1)! \mathrm{Im}\langle \hat{f}_{\mathbf{k},n} \hat{f}^*_{\mathbf{k},n+1}\rangle, \tag{7}$$

$$Q_i \equiv \frac{1}{2}\sum_{\mathbf{k}} k_y \int dv_\parallel (v_\parallel^2 - 1) \mathrm{Im}\langle \Psi_{\mathbf{k}} \tilde{f}_{-\mathbf{k},n=2}\rangle, \tag{8}$$

and $\delta_{n,m} = 1(n=m), 0(n\neq m)$. Here, Q_i denotes the turbulent ion heat flux downward in the temperature gradient. On the right-hand side of Eq. (5), $\eta_i Q_i$ represents the entropy production supplied at $n = 2$ while $-2\nu n \delta S_n$ is the collisional entropy dissipation term. We also find that $J_{n-1/2}$ $(J_{n+1/2})$ represents the entropy transfer from the $(n-1)$th $(n$th) to the nth $[(n+1)$th] Hermite-polynomial portion.

Now, let us investigate the entropy spectrum δS_n in the steady turbulence, where the left-hand side of Eq. (5) vanishes. Considering small scales in the velocity space ($n > 2$), we treat n as a continuous variable and use the approximation $J_{n+1/2} - J_{n-1/2} \simeq dJ_n/dn$ to obtain $dJ_n/dn = -2\nu n \delta S_n$. Assuming that the n-dependence of the phase of $\hat{f}_{\mathbf{k},n}$ is determined mainly by the phase mixing of the ballistic modes, we can put $\hat{f}_{\mathbf{k},n-1/2}\hat{f}^*_{\mathbf{k},n+1/2} \simeq i(k_y/|k_y|)|\hat{f}_{\mathbf{k},n}|^2$. Then, using Eqs. (4) and (6), we have $J_n/\delta S_n \simeq 2\Theta\sqrt{n}\langle|k_y|\rangle_n$, where the spectral average $\langle\cdots\rangle_n \equiv (\sum_{\mathbf{k}} \delta S_{\mathbf{k},n}\cdots)/(\sum_{\mathbf{k}} \delta S_{\mathbf{k},n})$ $\equiv (\sum_{\mathbf{k}}\langle|\hat{f}_{\mathbf{k},n}|^2\rangle\cdots)/(\sum_{\mathbf{k}}\langle|\hat{f}_{\mathbf{k},n}|^2\rangle)$ are defined. Using the relations shown above, we obtain

$$\frac{d}{dn}\left(2\Theta\sqrt{n}\langle|k_y|\rangle_n \delta S_n\right) = -2\nu\ n\ \delta S_n \qquad \text{for } n > 2. \tag{9}$$

In order to derive the functional form of δS_n, we still need to specify the n-dependence of $\langle|k_y|\rangle_n$ included in Eq. (9). For this purpose, we examine the role of $\mathbf{E}\times\mathbf{B}$ convection term in Eq. (3). Here, we point out the analogy of our problem to the study by Batchelor on the spectrum of the passive scalar for wave lengths smaller than the Kolmogorov scale in the large Prandtl number case [10]. Like the turbulent passive scalar in small scales, $\hat{f}_{\mathbf{k},n}$ for large n is considered to vary so rapidly that $\mathbf{E}\times\mathbf{B}$ flow acting on $\hat{f}_{\mathbf{k},n}$ is regarded as a steady one which is statistically independent of $\hat{f}_{\mathbf{k},n}$. Then, the strain of the steady flow causes the exponential growth of the wave number of the convected variable, $\mathbf{k} \propto e^{\gamma t}$ [10]. Under the phase-mixing process described by the second term in the left-hand side of Eq. (1), a factor in the form of $\exp(-iv_\parallel\Theta k_y/\gamma)$ is produced in the velocity distribution function. In the Hermite-polynomial expansion of this factor, components of order $n \simeq (\Theta k_y/\gamma)^2$ are dominant. Thus, we have the relation, $\Theta|k_y| \simeq \gamma\sqrt{n}$. Substituting this into Eq. (9) and integrating it with respect to n yield the entropy spectrum δS_n,

$$\delta S_n = \frac{\sigma}{2\gamma n}\exp\left(-\frac{\nu n}{\gamma}\right), \tag{10}$$

where $\sigma \equiv 2\nu\int_0^\infty n\delta S_n dn \simeq 2\nu\sum_n n\delta S_n$ represents the collisional entropy dissipation rate. In the steady state, the entropy dissipation and production rates balance with each other so that $\sigma = \eta_i Q_i$. We find from Eq. (10) that, in the range where neither entropy production nor collisional dissipation occurs ($2 < n \ll \gamma/\nu$), we expect the power-law of $\delta S_n \propto 1/n$ with $J_n = \sigma = $ const., which is analogous to the passive scalar spectrum ($\propto 1/k$) and its power transfer in the viscous-convective wave-number (k) subrange derived by Batchelor [10].

In the analytical treatment for derivation of Eq. (10), $\langle|k_y|\rangle_n \propto \sqrt{n}$ increases infinitely with n. However, in numerical simulations, there exists the upper limit of $|\mathbf{k}|$. Even if the potential amplitude is sufficiently damped at the maximum wave number in the simulation, still $f_{\mathbf{k},n}$ for large $|\mathbf{k}|$ and large n is continuously produced by the combination of the $\mathbf{E}\times\mathbf{B}$ convection and the phase mixing process. Therefore, saturation of $\langle|k_y|\rangle_n$ with increasing n is anticipated due to the upper limit of $|\mathbf{k}|$. In this case, taking $\Theta\langle|k_y|\rangle_n = \gamma_M$ as independent of n and using Eqs.(4) and (6), we obtain $J_n/\delta S_n = 2\gamma_M\sqrt{n}$ and

$$\delta S_n = \frac{\sigma}{2\gamma_M\sqrt{n}}\exp\left(-\frac{2}{3}\frac{\nu n^{3/2}}{\gamma_M}\right), \tag{11}$$

where σ is the same as given after Eq. (10).

Now, let us compare the above analytical results with numerical simulation results. Here, in order to get a significant anomalous transport level, we consider the case with

no flow component ($k_y = 0$) [3] and use parameters $(\eta_i, \Theta) = (10, 2.5)$ (The slab ITG turbulence with zonal flow is investigated in Ref. 2, where zonal flow generation and resultant turbulent transport suppression are found to be very strong compared with the toroidal case.) In Fig. 1, the spectrum-averaged wave number $\langle |k_y| \rangle_n$ is plotted as a function of n for $(k_{\max}, \nu) = (6.4, 2 \times 10^{-3})$ and for $(k_{\max}, \nu) = (12.8, 1.25 \times 10^{-4})$. We find that $\langle |k_y| \rangle_n$ grows nearly in proportional to $\sqrt{n}$ for smaller values of $n(> 2)$, which agrees with the estimate of $\Theta \langle |k_y| \rangle_n \simeq \gamma \sqrt{n}$ used for derivation of Eq. (10). Also, saturation of $\langle |k_y| \rangle_n$ for larger n due to the upper limit $k_{\max}$ is seen in Fig. 1. The saturation starts at lower n for smaller $k_{\max}$.

From the simulation result with $k_{\max} = 6.4$ (12.8) in Fig. 1, we obtain $\gamma \simeq 0.75$ (0.5) and $\sigma \simeq 63$ (36) for the spectral function in Eq. (10) while, for that in Eq. (11), we put $\gamma_M = 7.5$ (15). The entropy spectra δS_n obtained by the same simulation as in Fig. 1 are compared with those given by the combination of Eqs. (10) and (11) in Fig. 2, where we use Eq. (10) for $n < 3 \times 10^2$ (10^3) and Eq. (11) for $n > 3 \times 10^2$ (10^3) in the case of $k_{\max} = 6.4$ (12.8). In the dissipation range with large values of n, the spectrum found in the simulation is well fitted by Eq. (11). Since the constant factor in Eq. (10) is determined by the constraint $2\nu \int n \delta S_n dn = \sigma$ with σ evaluated from the simulation result, the spectrum δS_n for lower n evaluated from Eq. (10) becomes slightly smaller than that in the simulation in order to satisfy the constraint because, for higher n, the latter spectrum is smaller than the former due to the effect of finite $k_{\max}$. Thus, the entropy spectrum observed by the slab ITG turbulence simulation can be well explained by combining the analytical expressions in Eqs. (10) and (11). If we can employ an sufficiently high value of $k_{\max}$, the simulation will reproduce the spectrum δS_n in Eq. (10) for the whole range of $n > 2$.

3. TOROIDAL ITG TURBULENCE

In toroidal systems such as tokamaks and helical plasmas, the magnetic curvature combined with the ion temperature gradient drives instabilities, so-called toroidal ITG modes, which are considered responsible for anomalous ion heat transport in core plasma regions. In this section, we investigate anomalous transport and entropy balance in the toroidal ITG turbulence as well as zonal flows dynamics in toroidal systems based on the gyrokinetic theory and simulation [4].

3.1. Turbulent Transport and Entropy Balance in Tokamaks

Basic equations for the toroidal ITG turbulence are given by the ion gyrokinetic equation [11] for the perturbed gyrocenter distribution function $\delta f(\mathbf{x}, v_\parallel, \mu, t) = f - F_M$,

$$\frac{\partial \delta f}{\partial t} + \left(v_\parallel \mathbf{b} + \mathbf{v}_d + \frac{c}{B_0} \mathbf{b} \times \nabla \Psi \right) \cdot \nabla \left(F_M + \delta f \right) = C_i(\delta f) \tag{12}$$

and the quasineutrality condition which is written in the wave number (k_x, k_y) space as

$$\int d^3 v J_0(k_\perp v_\perp / \Omega_i) \delta f_{k_x,k_y} - n_0 \frac{e \phi_{k_x,k_y}}{T_i} [1 - \Gamma_0(b_\mathbf{k})] = \frac{e}{T_e} [\phi_{k_x,k_y} - \langle \phi_{k_x,k_y} \rangle \delta_{k_y,0}] \tag{13}$$

where $\Gamma_0(b_\mathbf{k}) \equiv I_0(b_\mathbf{k}) \exp(-b_\mathbf{k})$, $b_\mathbf{k} \equiv k_\perp^2 T_i / (m_i \Omega_i)$, and $\langle \cdots \rangle$ represents the flux surface average. In Eq. (12), $\mathbf{v}_d$ denotes the toroidal drift velocity, Ψ is the gyrophase-averaged potential defined by $\Psi_{k_x,k_y} = J_0(k_\perp v_\perp / \Omega_i) \phi_{k_x,k_y}$ in the (k_x, k_y) space, and $C_i(\delta f)$ is

given in the gyrophase-averaged form of the Lenard-Bernstein collision operator. Here, we use the toroidal flux tube coordinates $x = r - r_0$, $y = (r_0/q_0)(q\theta - \zeta)$, and $z = \theta$, where r, θ, ζ, and q are the minor radius, the poloidal angle, the toroidal angle, and the safety factor, respectively [12]. The flux tube is set around the flux surface $r = r_0$ with the safety factor $q = q_0$. The square of the perpendicular wave number is given by $k_\perp^2 = (k_x + \hat{s}k_y z)^2 + k_y^2$ where $\hat{s} = (r_0/q_0)(dq/dr)_{r=r_0}$ is the magnetic shear parameter.

In the same manner as in the case of the slab ITG turbulence (see Sec. 2 and Ref. 3), we normalize physical variables and derive the entropy balance equation for the toroidal ITG turbulence which is written in the flux-surface-averaged form (also integrated in the velocity space) as

$$\frac{d}{dt}(\delta S + W) = \eta_i Q_i + D_i \tag{14}$$

where the entropy variable δS, the potential energy W, the ion heat flux Q_i, and the collisional dissipation D_i are defined by

$$\begin{aligned}
\delta S &= \sum_{k_x,k_y} \delta S_{k_x,k_y} = \frac{1}{2}\sum_{k_x,k_y} \left\langle \int \frac{|f_{k_x,k_y}|^2}{F_M} d^3v \right\rangle \\
W &= \sum_{k_x,k_y} W_{k_x,k_y} = \frac{1}{2}\sum_{k_x,k_y} \left[\left\langle (1 - \Gamma_0 + \tau)|\phi_{k_x,k_y}|^2 \right\rangle - \tau |\left\langle \phi_{k_x,k_y} \right\rangle|^2 \delta_{k_y,0} \right] \\
Q_i &= \sum_{k_x,k_y} Q_{i,k_x,k_y} = \frac{1}{2}\sum_{k_x,k_y} \left\langle i k_y \phi_{-k_x,-k_y} \int v^2 J_0 f_{k_x,k_y} d^3v \right\rangle \\
D_i &= \sum_{k_x,k_y} D_{i,k_x,k_y} = \sum_{k_x,k_y} \left\langle \int \left[\left(J_0 \phi_{-k_x,-k_y} + \frac{f_{-k_x,-k_y}}{F_M} \right) C\left(f_{k_x,k_y}\right) \right] d^3v \right\rangle
\end{aligned} \tag{15}$$

respectively.

In Fig. 3 (a), the ion thermal diffusivity χ_i is shown as a function of time obtained from the Eulerian gyrokinetic simulation of the toroidal ITG turbulence [4]. Here, the Cyclone DIII-D base case parameters [13] ($R_0/L_T = 6.92$, $\epsilon_t \equiv r_0/R_0 = 0.18$, $r_0/\rho_i = 80$, $\hat{s} = 0.78$, $q_0 = 1.4$, $\eta_i = 3.114$, and $T_i/T_e = 1$) are used. We find the time-averaged ion thermal diffusivity $\chi_i \simeq 1.4\rho_i^2 v_{ti}/L_n$ for $200 < v_{ti}t/L_n < 250$ in the saturated turbulent state, which is comparable with those of other gyrokinetic simulations done by using the same parameters ($\chi_{\simeq} 2\rho_i^2 v_{ti}/L_n$) [13]. Figure 3 (b) shows how entropy balance is satisfied in the same gyrokinetic simulation as in Fig. 3 (a). We see that the entropy balance equation is accurately satisfied owing to high phase-space resolution in the simulation and that the saturated (or steady) turbulent state is characterized by the balance between the turbulence entropy production due to the ion thermal transport in the ion temperature gradient and the collisional dissipation, $\eta_i Q_i \simeq -D_i$. In this balance, the ion thermal transport or the entropy production is associated with the macroscopic structure of the velocity-distribution function while the collisional dissipation occurs in the microscopic velocity scales. This implies that the entropy is transferred from the macroscopic to micro scales in the velocity space as seen in Sec. 2 for the case of the slab ITG turbulence. Spectral analysis for the velocity distribution function in the toroidal ITG turbulence remains as a future task to detailedly investigate the entropy spectrum and its transfer process.

3.2. Zonal Flow Dynamics in Tokamaks and Helical Plasmas

Since plasma turbulence and transport are significantly reduced in the existence of zonal $\mathbf{E}\times\mathbf{B}$ flows [6], it is critically important to study zonal flow dynamics in toroidal configurations. According to Rosenbluth and Hinton [14], for tokamaks, the ratio of the flux-surface-averaged electrostatic potential $\langle\phi_{\mathbf{k}}(t)\rangle$ to the initial perturbation $\langle\phi_{\mathbf{k}}(0)\rangle$ with $\mathbf{k}=k_r\nabla r$ is given by

$$\frac{\langle\phi_{\mathbf{k}}(t)\rangle}{\langle\phi_{\mathbf{k}}(0)\rangle}=\frac{1}{1+1.6q^2/\sqrt{\epsilon_t}} \tag{16}$$

where $\epsilon_t=r/R_0$ (r: the minor radius, R_0: the major radius) is the inverse aspect ratio. The term $1.6q^2/\sqrt{\epsilon_t}$ in the denominator of the right-hand side in Eq. (16) represents shielding by neoclassical polarization. Equation (16) is interpreted as a linear response $\langle\phi_{\mathbf{k}}(t)\rangle$ to a source in the of form of the delta function $\sim\delta(t)$ which is equivalent to a kernel in the integral equation relating $\langle\phi_{\mathbf{k}}(t)\rangle$ to a time-dependent source function $S_{\mathbf{k}}(t)$ [14].

Figure 4 (a) shows time evolution of the zonal flow potential obtained by the gyrokinetic simulation for the collisionless case where nonlinear source terms for zonal flow generation are dropped. Here, $k_r\rho_i=0.1715$ and the Cyclone DIII-D base case parameters [13] ($R_0/L_T=6.92$, $\epsilon_t\equiv r/R_0=0.18$, $r/\rho_i=80$, $\hat{s}=0.78$, $q=1.4$ and $T_i/T_e=1$) are used again. We can see that, as oscillations due to the geodesic acoustic mode (GAM) [15] are damped, the potential amplitude approaches the value predicted by Eq. (16). In Fig. 4 (b), contours of the real part of the perturbed distribution function on the $(v_\parallel,v_\perp)$-space at $\theta=0$ (corresponding to the outermost position in the toroid) are plotted for $v_{ti}t/L_n=50$ in the same simulation as in Fig. 4 (a). A distinct difference between characteristics of passing and trapped particle distributions is found in Fig. 4 (b). Striped patterns appearing in the passing particle region represent the parallel phase mixing which causes damping of the GAM oscillations while more coherent structures seen in the trapped particle region reflect the neoclassical polarization associated with banana orbits.

Now, let us consider helical systems with the magnetic field strength given by

$$B=B_0[1-\epsilon_t\cos\theta-\epsilon_h\cos(L\theta-M\zeta)] \tag{17}$$

where B_0 is the magnitude on the magnetic axis and M (L) is the toroidal (main poloidal) period number of the helical field. For the Large Helical Device (LHD) [16], $L=2$ and $M=10$. Here, we assume that $lq/M\ll 1$. As shown by Shaing and Hokin [17], multiple-helicity effects can be included by regarding ϵ_h as a function of θ.

In the same manner as in Rosenbluth and Hinton deriving Eq. (16), we hereafter treat a response of zonal flow to an initial perturbation on a time scale much longer than a bounce period of trapped particles but shorter than an effective collision time. Bounce-averaged positions of particles trapped in helical ripples generally move across magnetic surfaces in contrast to banana centers of trapped particles in tokamaks which stay still in the collisionless case. These radial drift motions of helically trapped particles cause neoclassical ripple transport in the weak collisionality regime. Here we investigate effects of helically trapped particles on collisionless zonal flow dynamics. The area of helically trapped particles on the velocity space is nearly proportional to $\sqrt{\epsilon_h}$. It is shown from the gyrokinetic equation that the nonadiabatic part of the helically trapped particle density are damped through the collisionless phase mixing process

associated with the bounce-averaged radial drift on a long time scale, $t \gg 1/|k_r\langle v_{dr}\rangle_b|$, where $\langle v_{dr}\rangle_b$ denotes the bounce-averaged radial drift velocity of helically trapped particles. On the other hand, effects of the bounce-averaged radial drift are not significant on a short time scale, $t \ll 1/|k_r\langle v_{dr}\rangle_b|$. The ratio of the zonal flow potential to the initial perturbation for the helical system is derived from the solution of the gyrokinetic equation and the quasineutrality condition as

$$\frac{\langle\phi_{\mathbf{k}}(t)\rangle}{\langle\phi_{\mathbf{k}}(0)\rangle} = \begin{cases} \dfrac{1}{1+q^2F(\epsilon_t,\epsilon_h)} & (\text{for } t \ll 1/|k_r\langle v_{dr}\rangle_b|) \\ \dfrac{(k_r\rho_i)^2[1-(2/\pi)\langle(2\epsilon_h)^{1/2}\rangle]}{(k_r\rho_i)^2[1-(2/\pi)\langle(2\epsilon_h)^{1/2}\rangle+q^2F(\epsilon_t,\epsilon_h)]+(2/\pi)\langle(2\epsilon_h)^{1/2}\rangle(1+T_i/T_e)} & \\ & (\text{for } t \gg 1/|k_r\langle v_{dr}\rangle_b|) \end{cases} \tag{18}$$

where $q^2F(\epsilon_t,\epsilon_h)$ represents a contribution from neoclassical polarization due to toroidally trapped particles similar to $1.6q^2/\epsilon_t^{1/2}$ in Eq. (16) [a complicated functional form of $F(\epsilon_t,\epsilon_h)$ is not shown here]. In the right-hand side of Eq. (18), terms proportional to $\epsilon_h^{1/2}$ are derived from suppression of the nonadiabatic density perturbation due to the bounce-averaged radial drift of helically trapped particles and a term with T_i/T_e represents a contribution from the helically trapped electron density. For evaluating the transition time $1/|k_r\langle v_{dr}\rangle_b|$ in Eq. (18), the particle velocity and the poloidal angle included in $\langle v_{dr}\rangle_b$ are given by the thermal velocity v_t and $\theta \sim \pi/2$, respectively. In the limit of $\epsilon_h \to +0$, we find that $F(\epsilon_t,\epsilon_h) \to 1.6\epsilon_t^{-1/2}$ and that Eq. (18) coincides with the Rosenbluth-Hinton formula in Eq. (16).

Time evolution of the zonal flow potential in the helical system for $L = 2$, $M = 10$, $q = 1.5$, $\epsilon_t = 0.1$ and $\epsilon_h = 0.1$ is shown in Figs. 5 (a) and (b). Here, the single-helicity case is considered (ϵ_h is independent of θ). Normalized radial wave numbers $k_r\rho_i = 0.13$ and $k_r\rho_i = 0.20$ are used in Figs. 5 (a) and (b), respectively. Solid curves are results from the gyrokinetic simulation while horizontal lines are given by Eq. (18) for $t < 1/|k_r\langle v_{dr}\rangle_b|$ and $t > 1/|k_r\langle v_{dr}\rangle_b|$. It is seen that, after the GAM oscillations are damped, the zonal flow amplitudes approaches theoretically predicted values. Since the helically trapped electron density are not treated in the present simulation, the term proportional to T_i/T_e in Eq. (18) is dropped when comparing the theory with the simulation results in Figs. 5 (a) and (b).

Equation (18) contains the radial wave number dependence of the zonal flow potential for $t \gg 1/|k_r\langle v_{dr}\rangle_b|$, which is not found in Eq. (16) for tokamak cases. We see from Eq. (18),that, for the longer radial wave lengths, the zonal flow potential amplitude in the long time limit decreases although simultaneously the transition time $1/|k_r\langle v_{dr}\rangle_b|$, in which the radial wave number dependence appears, becomes longer. It should be noted that some optimization of multiple-helicity configuration with $\epsilon_h = \epsilon_h(\theta)$ can reduce $|\langle v_{dr}\rangle_b|$ and $F(\epsilon_t,\epsilon_h)$, which implies that a large zonal flow amplitude can be maintained for a long time by choosing an appropriate helical magnetic configuration. Comparisons between our theory and simulation results for multiple-helicity cases still remain as a future study. Furthermore, since Eqs. (16) and (18) both represent the response of the zonal flow potential, we should apply these theoretical results to analyses of the zonal flow generation mechanism in the toroidal ITG turbulence which is also an important future task.

4. CONCLUSIONS

In the present paper, kinetic properties in the slab and toroidal ITG turbulence are investigated by using analytical theories and high-resolution Eulerian kinetic simulations which directly solve phase-space structures of the particle distribution function. By a spectral analysis of the distribution function for the slab ITG turbulence, the turbulence entropy production, transfer, and dissipation processes are elucidated and the analytically derived entropy spectral functions agree with the simulation results. Our Eulerian gyrokinetic simulation of the toroidal ITG turbulence is shown to accurately satisfy the entropy balance equation and give the reliable ion thermal diffusivity in the steady turbulent state where the balance between the entropy production by the ion thermal transport in the temperature gradient and the collisional dissipation is confirmed. A formula for collisionless time evolution of the zonal flow potential in helical systems, which reduces to the formula by Rosenbluth and Hinton in the axisymmetric limit, is analytically derived and its validity is verified by the gyrokinetic simulation.

ACKNOWLEDGMENTS

This work is supported in part by the Japanese Ministry of Education, Culture, Sports, Science, and Technology, Grant Nos. 16560727 and 14780387.

REFERENCES

[1] H. Sugama, T.-H. Watanabe, and W. Horton, Phys. Plasmas **10**, 726 (2003).
[2] T.-H. Watanabe and H. Sugama, Phys. Plasmas **9**, 3659 (2002).
[3] T.-H. Watanabe and H. Sugama, Phys. Plasmas **11**, 1476 (2004).
[4] T.-H. Watanabe and H. Sugama, 20th IAEA Fusion Energy Conference (Vilamoura, Portugal, 2004) TH/8-3Rb.
[5] W. Horton, Rev. Mod. Phys. **71**, 735 (1999).
[6] P. W. Terry, Rev. Mod. Phys. **72**, 109 (2000).
[7] J. A. Krommes and G. Hu, Phys. Plasmas **1**, 3211 (1994).
[8] H. Sugama and W. Horton, Phys. Plasmas **2**, 2989 (1995).
[9] H. Sugama, M. Okamoto, W. Horton, and M. Wakatani, Phys. Plasmas **3**, 2379 (1996).
[10] G. K. Batchelor, J. Fluid Mech. **5**, 113 (1959).
[11] E. A. Frieman and L. Chen, Phys. Fluids **25**, 502 (1982).
[12] M. A. Beer, S. C. Cowley, G. W. Hammett, Phys. Plasmas **2**, 2687 (1995).
[13] A. M. Dimits, *et al.*, Phys. Plasmas **7**, 969 (2000).
[14] R. M. Rosenbluth and F. L. Hinton, Phys. Rev. Lett. **80**, 724 (1998).
[15] N. Winsor, J. L. Johnson, and J. J. Dawson, Phys. Fluids **11**, 2248 (1968).
[16] O. Motojima, *et al.*, Nucl. Fusion **43**, 1674 (2003).
[17] K. C. Shaing and S. A. Hokin, Phys. Fluids **26**, 2136 (1983).

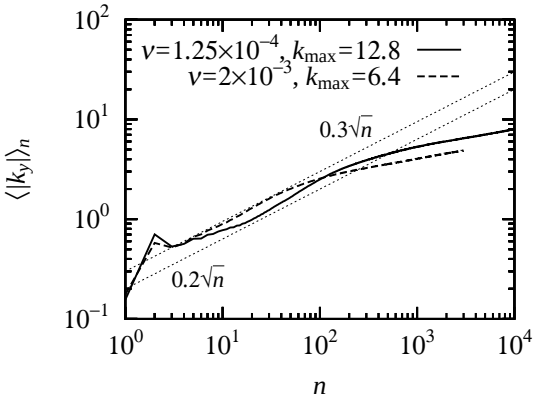

Fig. 1. Spectrum-averaged wave number $\langle|k_y|\rangle_n$ for $(k_{\max}, \nu) = (6.4, 2 \times 10^{-3})$ and $(k_{\max}, \nu) = (12.8, 1.25 \times 10^{-4})$. Upper and lower dotted straight lines represent $\langle|k_y|\rangle_n = 0.3\sqrt{n}$ and $0.2\sqrt{n}$, respectively.

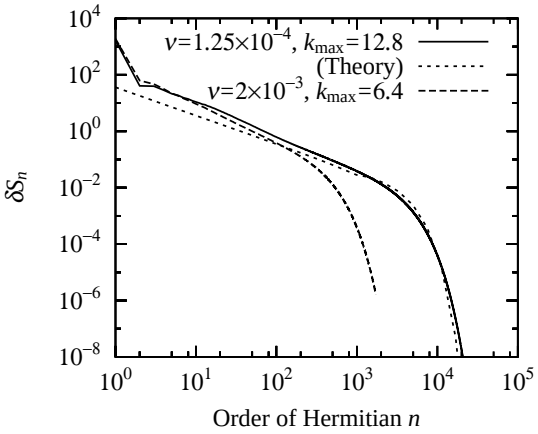

Fig. 2. Entropy spectra δS_n (solid and dashed lines) obtained by the same simulation as in Fig. 1. For comparison, dotted and dot-dashed lines represent the combination of Eqs. (10) and (11). Here, Eq. (10) is used for $n < 3 \times 10^2$ (10^3) and Eq. (11) for $n > 3 \times 10^2$ (10^3) in the case of $k_{\max} = 6.4$ (12.8).

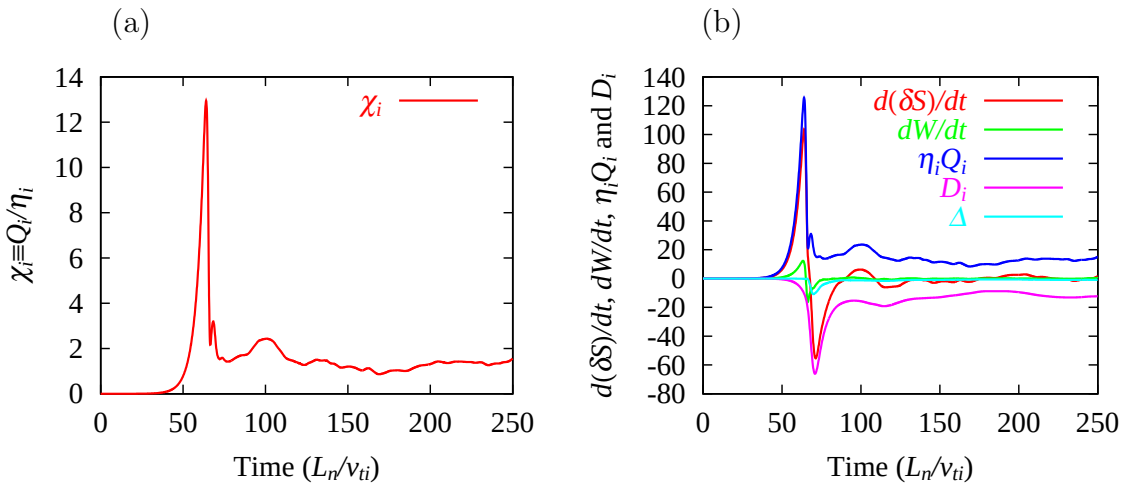

Fig. 3. Time evolution of the ion themal diffusivity (a) and the terms in the entropy balance equation (b) [See Eq. (14)] obtained by the toroidal ITG turbulence simulation.

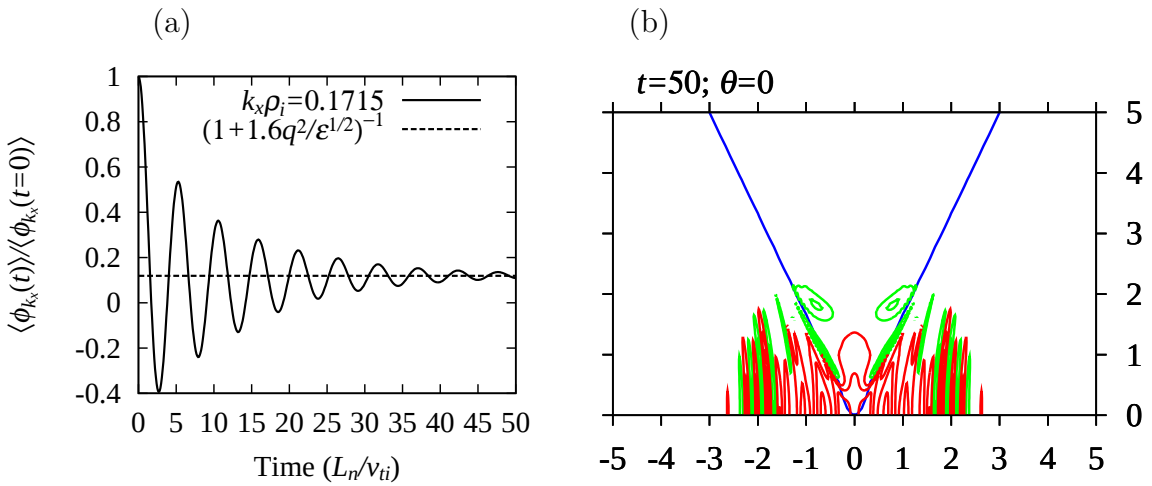

Fig. 4. Time evolution of the zonal flow potential (a) and contours of the real part of the perturbed distribution function on the $(v_\parallel, v_\perp)$-space for $v_{ti}t/L_n = 50$ (b) for a tokamak obtained by the gyrokinetic simulation. A horizontal dotted line in (a) corresponds to the Rosenbluth-Hinton theory. Blue straight lines in (b) show the boundaries between trapped and passing particle regions.

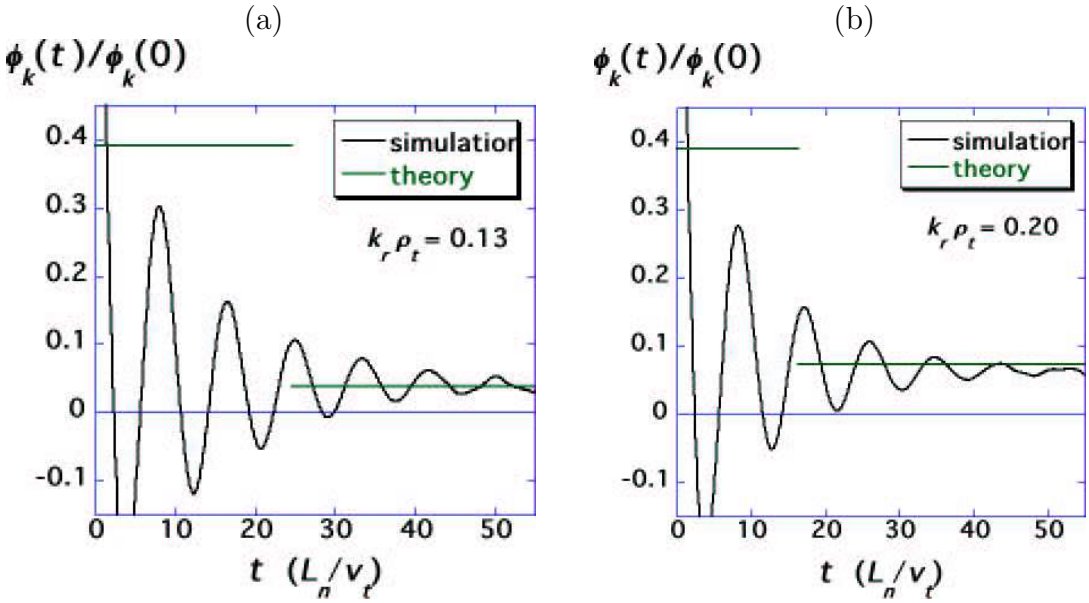

Fig. 5. Time evolution of the zonal flow potential in a helical system with $L = 2$, $M = 10$, $q = 1.5$, and $\epsilon_t = \epsilon_h = 0.1$ for $k_r\rho_i = 0.13$ (a) and $k_r\rho_i = 0.20$ (b) obtained by the gyrokinetic simulation. Horizontal lines are given by Eq. (18).